JOURNAL OF MATERIALS SCIENCE **38** (2003) 3211 – 3217

Preparation of lead titanate ultrafine powders from combined polymerisation and pyrolysis route

E. ERDEM, R. BÖTTCHER, H.-C. SEMMELHACK
Institut für Experimentelle Physik II, Universität Leipzig, D-04103 Leipzig, Germany

H.-J. GLÄSEL, E. HARTMANN, D. HIRSCH
Institut für Oberflächenmodifizierung, D-04318 Leipzig, Germany
E-mail: hartmann@rz.uni-leipzig.de

Lead titanate ($PbTiO_3$) nanopowders were prepared from a monomeric metallo-organic precursor through combined solid-state polymerisation and pyrolysis (CPP). This makes it possible to adjust the mean particle size in a wide range by just choosing the appropriate reaction temperature. This particular preparation route was studied by thermogravimetric analysis (TGA) and differential scanning calorimetry (DSC). The size effects in the resulting $PbTiO_3$ nanopowders were investigated by standard methods such as X-ray diffraction (XRD) and FT-Raman spectroscopy. By using the double Voigt method in analysing the XRD results, smaller mean particle size and narrower size distributions were found for powders prepared at lower reaction temperatures, with the tetragonality being reduced. Preliminary electron paramagnetic resonance (EPR) measurements demonstrate that paramagnetic chromium probe ions incorporate very well into the $PbTiO_3$ lattice, particularly enabling corresponding high-field EPR measurements which have proven exceedingly informative in our previous investigations on Mn^{2+}-doped barium titanate ($BaTiO_3$) nanopowders. Moreover, the potential of the CPP route is enhanced to prepare perovskitic stoichiometric solutions for advanced practical applications.

1. Introduction

The continuous studies of size effects on ferroelectric properties since the fifties have obtained great impetus in recent years [1]. Curie temperature, electrical polarization, coercive field, switching time etc. potentially depend on particle size or, more generally, correlational length [2].

At first, the main focus was set on barium titanate ($BaTiO_3$) which is the representative prototype of the perovskite materials and, moreover, is most widely used in the capacitor industry. Due to small internal stress, the tetragonal phase is less stabilised than in lead titanate ($PbTiO_3$) and the tetragonal-to-cubic ferroelectric-to-paraelectric phase transition at 120°C is readily accessible in all common spectroscopic studies. In addition to this, the small stress mediates further structural transformations (rhombohedral-to-orthorhombic and orthorhombic-to-tetragonal at −90°C and 5°C, respectively) which makes $BaTiO_3$ exceedingly attractive for spectroscopic investigations, particularly for electron paramagnetic resonance (EPR) studies (of course, after corresponding doping by paramagnetic probe ions such as Mn^{2+}, Gd^{3+} or Cr^{3+}) [3]. The application of various spectroscopic techniques such as Raman spectroscopy [4], X-ray absorption spectroscopy (XANES) [5] and EPR [6] to ultrafine $BaTiO_3$ powder samples, enabled us to devise a detailed idea according to which a $BaTiO_3$ particle consists of a regular tetragonal core and a distorted surface layer. While the latter shell reveals largely size-independent features, the core undergoes a size-driven transition into the cubic paraelectric phase. These previous investigations on $BaTiO_3$ nanopowders were based on the combined polymerisation and pyrolysis (CPP) of metallo-organic precursors which yielded high-quality $BaTiO_3$ nanopowders in the broad size range between 10 nm and 1.5 μm by just choosing appropriate reaction temperature (600°C up to 1350°C) and atmosphere (inert or oxidative) [7].

The preparation of ultrafine $PbTiO_3$ powders in the present work is not just a simple retake of the former $BaTiO_3$ route. Rather, both preparative and solid-state aspects exist which make the $BaTiO_3$ and $PbTiO_3$ cases very different. At high temperatures difficulties may arise with the volatility of the intermediary lead oxide PbO. In addition, tempering under inert conditions appears inapplicable in a decisive initial stage of particle formation because PbO might be readily reduced to metallic lead. The rather high internal stress in $PbTiO_3$ increases relevant parameters such as the spontaneous polarization. This not only potentially enhances the technological relevance of the $PbTiO_3$

ferroelectrics but the inherent high internal stress complicates the preparation and handling of this material to such an extent that one has to resort to powder technology. Furthermore, the high internal stress and resulting strong stabilization of the tetragonal phase entail the high ferroelectric-to-paraelectric phase transition temperature at 493°C which is difficult to access in spectroscopic studies. However, the occurrence of an orthorhombic phase in $PbTiO_3$ nanopowders (with mean particle size d_m of about 7 nm below 166°C, [8]) has directed new attention to preparatory work in the size region below 10 nm, particularly by employing template synthesis [9] and micellar microemulsion routes [10, 11]. It should be also mentioned that inorganic-organic nanocomposites can be obtained in a direct way by applying a modified CPP route [7], with the temperature chosen so low that pyrolysis is precluded. Thus, Yogo *et al.* [12] prepared at a reaction temperature of 100°C nanoscalic $PbTiO_3$ inclusions in a polymeric matrix.

By just starting from adequate mixtures of metallo-organic precursors, the CPP preparation route can yield perovskitic stoichiometric solutions and modifications in a particularly unconstrained way (for respective actual studies of such materials, see [13–17]). A special advantageous feature of the CPP preparation is its ability to introduce paramagnetic probe ions (first of all Gd^{3+}, Mn^{2+} and Cr^{3+}). Previous investigations were based on Mn^{2+} probe ions, disclosing pronounced size effects on the ferroelectric behaviour of $BaTiO_3$ nanopowders [6]. However, doping the ultrafine $PbTiO_3$ powders by chromium ions appears more appropriate here: In X-band EPR measurements of Cr^{3+}-doped $PbTiO_3$ single crystals strong configurational instabilities were detected [18], and extension of this work to ultrafine powder samples and high-field EPR measurements appears rather promising. In such an endeavour, great effort is to be invested to extend the mean particle size range to small values below a critical value d_{crit} of presumably less than 10 nm.

2. Experimental

2.1. $PbTiO_3$ nanopowder preparation

The CPP preparation route took part of its pattern from a literature recipe for synthesising nanoferrites [19] and consists of two consecutive steps: (a) preparation of the metallo-organic precursor and (b) combined solid-state polymerisation and pyrolysis. To prepare ferroelectric composites the ferroelectric particles must not be chosen arbitrarily small because in the finest nanoparticles the ferroelectricity as a collective long-range phenomenon may be lost due to the size-driven phase transition into the paraelectric phase ([1] and refs. cited therein). In the preparation high-purity *Aldrich* chemicals were used: lead(II) oxide PbO, titanium(IV) isopropoxide $Ti(O{-}C_3H_7)_4$ and methacrylic acid $CH_2{=}C(CH_3){-}COOH$. For EPR measurements chromium(III) acetylacetonate $Cr(CH_3COCH{=}C(OH)CH_3)_3$ was employed as dopant to yield a typical Cr^{3+} concentration of 5×10^{18} spins/g in the final powder sample. This is at variance to former procedures where the corresponding metal acetates were added as dopants [7]. However, chromium acetates of definite composition are not available so that we resorted to the acetylacetonate as substitute.

2.1.1. Metallo-organic precursor

A complex lead titaniumoxy methacrylate was obtained as a monomeric metallo-organic precursor from lead oxide, titanium(IV) isopropoxide and methacrylic acid in boiling pure chloroform (3 h magnetic stirring, 61°C) by four reactions as described below. 4-methoxyphenol (200 ppm) was added to the solution as stabiliser to avoid polymerisation of methacrylic acid during the heating. The following reactions take place subsequently:

$$PbO + 2\,CH_2{=}C(CH_3){-}COOH \rightarrow Pb(OOC{-}C(CH_3){=}CH_2)_2 + H_2O \quad (1)$$

$$Ti(O{-}C_3H_7)_4 + CH_2{=}C(CH_3){-}COOH \rightarrow Ti(O{-}C_3H_7)_3(OOC{-}C(CH_3){=}CH_2) + C_3H_7OH \quad (2)$$

$$2\,Pb(OOC{-}C(CH_3){=}CH_2)_2 + 2\,Ti(O{-}C_3H_7)_3(OOC{-}C(CH_3){=}CH_2) \rightarrow Pb_2Ti_2(O{-}C_3H_7)_6(OOC{-}C(CH_3){=}CH_2)_6 \quad (3)$$

Finally, the metallo-organic precursor is obtained:

$$Pb_2Ti_2(O{-}C_3H_7)_6(OOC{-}C(CH_3){=}CH_2)_6 + 3\,H_2O \rightarrow Pb_2Ti_2O_3(OOC{-}C(CH_3){=}CH_2)_6 + 6\,C_3H_7OH \quad (4)$$

After magnetic stirring the precursor solution was placed for drying into an oven (2 days, 70°C). The dry precursor was then carefully pulverised.

2.1.2. Polymerisation and pyrolysis

This process is rather complex and was studied by means of thermogravimetric analyses (TGA, using Perkin-Elmer TGA 7) and differential scanning calorimetric measurements (DSC, Perkin-Elmer DSC 7 analyser). The tempering process may be described by three reactions

$$n\,Pb_2Ti_2O_3(OOC{-}C(CH_3){=}CH_2)_6 \rightarrow [Pb_2Ti_2O_x(OOC{-}C(CH_3){-}CH_2)_y]_n + C + \textit{volatiles} \quad (5)$$

Under oxidative atmosphere (air) the shoulder in the TGA plot occurring at about 260°C (cf. Fig. 1) furnishes indication of the definite metallo-organic polymer $[Pb_2Ti_2O_5(OOC{-}C(CH_3){-}CH_2)_2]_n$ as an intermediate in the complex polymerisation/pyrolysis process which, finally, is followed by the nucleation step

$$[Pb_2Ti_2O_x(OOC{-}C(CH_3){-}CH_2)_y]_n \rightarrow PbCO_3 + TiO_2 + C + \textit{volatiles} \quad (6)$$

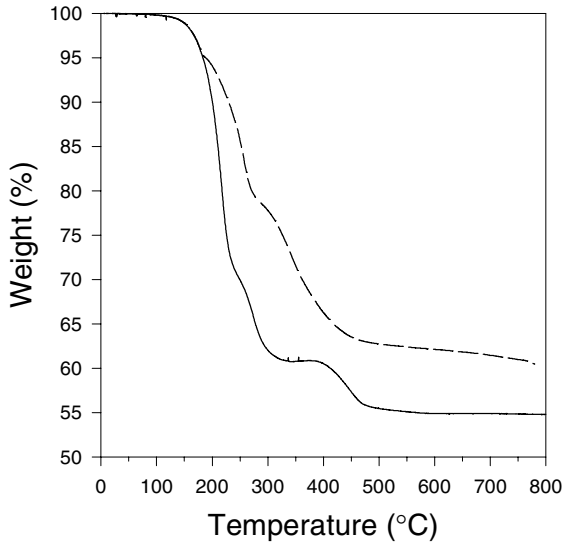

Figure 1 TGA of the $PbTiO_3$ powder formation in the CPP route (heating rate 10 K/min, under air-solid curve, N_2-broken).

The pronounced mass loss above 380°C is due to the solid-state reaction

$$PbCO_3 + TiO_2 \rightarrow PbTiO_3 + CO_2 \qquad (7)$$

which indeed may be verified by a simple stoichiometric consideration (for the analogous consideration of the $BaTiO_3$ case, see [5]).

Under inert atmosphere (N_2) the definite-polymer shoulder is temperature retarded by about 70 K and the nucleation and $PbTiO_3$ formation processes are largely prevented by incomplete char removal and, even more so, reduction of lead compounds to metallic lead. Hence, at variance to former CPP preparation of $BaTiO_3$ nanopowders [7], $PbTiO_3$ particles cannot be obtained under non-oxidative conditions.

In accordance with TGA in Fig. 1 the DSC measurements (cp. Fig. 2) show that under ambient air the solid-state polymerisation and concomitant pyrolysis (5, 6) proceed simultaneously at temperatures above 165°C.

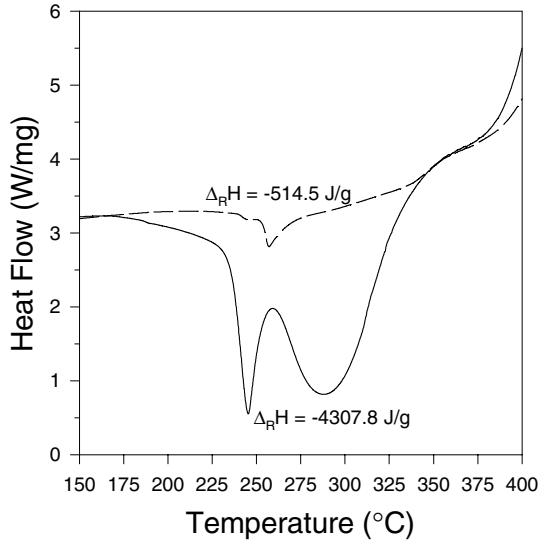

Figure 2 The same as in Fig. 1 for DSC.

Obviously, in determining the reaction enthalpy $\Delta_R H$, the oxidative processes dominate the polymerisation. Using the heat of combustion of methacrylic acid [20], the corresponding estimate for the combustion of the precursor was found to be −9670 J/g which considerably exceeds the measuring value of −4308 J/g. This finding may be attributed to incomplete combustion of some exhaust-gas components. The relative stability of the definite $[Pb_2Ti_2O_5(OOC{-}C(CH_3){=}CH_2)_2]_n$ precursor became manifest in the TGA shoulder at about 260°C which corresponds with the relative heat flow maximum occurring in the DSC graph at this particular temperature. Note that even under inert atmosphere the polymerisation enthalpy [20] falls short the measured value (−281 J/g vs. −514 J/g), evidencing non-oxidative pyrolytic (coking) processes.

One important problem in producing $PbTiO_3$ by the CPP route is the potential loss of PbO due to its significant vapour pressure at higher processing temperature. Therefore the stoichiometry was carefully checked by means of energy-dispersive X-ray spectroscopy (EDX).

2.2. Characterisation

SEM images were obtained at 30 keV using a JEOL JSM-6600 instrument. Electron-excited X-ray spectra (EDX) were recorded at 20 keV using a RÖNTEC EDWIN EDX system attached to the SEM. In order to prevent secondary X-ray excitation in the EDX measurements the insulating samples were coated with a 10 nm thick carbon layer using a LEYBOLD Z 400 sputter deposition coater. This layer contributes only less than 10% to the C K_α line.

XRD investigations were carried out at room temperature with a powder diffractometer (Philips X Pert) in Bragg-Brentano configuration, using Cu K_α radiation. FT-Raman spectra of the $PbTiO_3$ nanopowders with varying particle size and preparation temperatures were recorded using the Bruker RFS 100 spectrometer. The Nd: YAG laser was used as the excitation source at a power level of up to 30 mW. The measurements were done in the frequency range of 50 cm^{-1}–900 cm^{-1}.

Also, the possibility is worth mentioning to obtain inorganic-organic nanocomposites in a direct way by applying a modified CPP route [7], with the temperature chosen so low that pyrolysis is precluded. Thus, Yogo *et al.* [12] prepared at a reaction temperature of 100°C nanoscalic $PbTiO_3$ inclusions in a polymeric matrix.

3. Results and discussion

The SEM image in Fig. 3 shows $PbTiO_3$ nanoparticles as CPP-prepared at 900°C. They reveal a rather good surface morphology and their apparent mean particle size d_m apparently lies around 200 nm.

The EDX spectrum in Fig. 4 taken from the $PbTiO_3$ nanopowders reveals well-resolved Pb L, Ti K as well as Pb M X-ray lines. Spectrum analysis was done with the aid of the RÖNTEC EDWIN software, testifying proper stoichiometry and powder purity.

The XRD patterns of $PbTiO_3$ powder samples as CPP-prepared at lowest temperature (320°C) do not

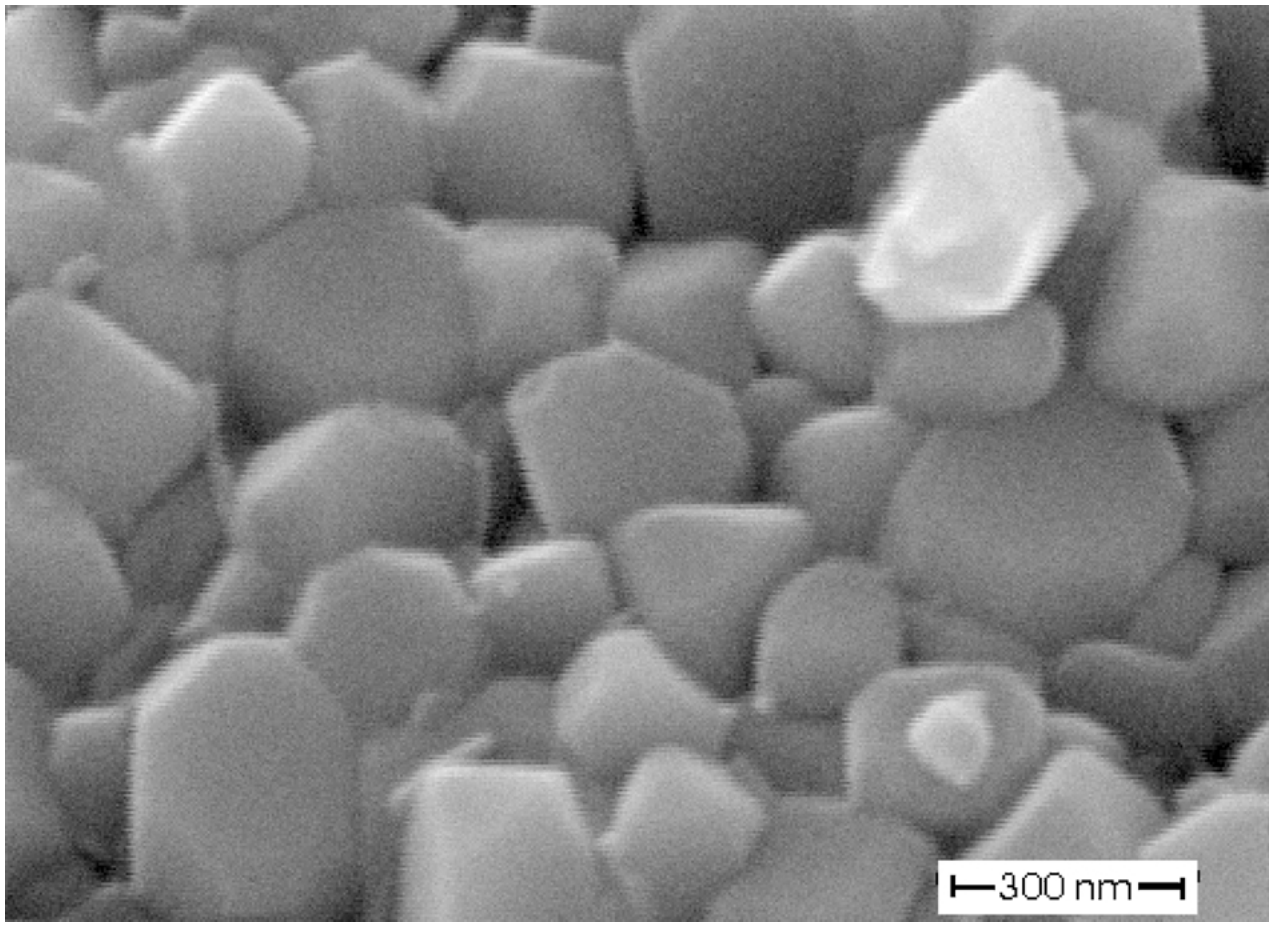

Figure 3 Scanning electron micrograph of chromium doped $PbTiO_3$ particles (CPP-prepared at 900°C).

reveal any sharp Bragg reflections (cf. Fig. 5), thus furnishing indication of amorphous state. Nanocrystallinity occurs in $PbTiO_3$ samples fabricated above 350°C. The XRD peaks are increasingly broadened with decreasing preparation temperature so that the $K_{\alpha 1}/K_{\alpha 2}$ splitting is not detectable. From the obvious broadening of the Bragg reflections or, more precisely, from the line shape of these peaks the crystallite size can be determined. A powerful procedure is the integral breadth method implemented in the computer software by Balzar [21]. The (111) and (222) reflections were fitted by Voigt functions with the aid of the Shadow software [22] and then, by the application of the integral-breadth method, both the surface and volume weighted column lengths, $\langle L \rangle_{vol}$ and $\langle L \rangle_{area}$, are estimated according to the "double-Voigt" method [23], with the latter being largely equivalent to the Warren-Averbach approach. Then, a rather complex averaging yields the surface or volume weighted particle sizes $\langle d \rangle_{area}$ and $\langle d \rangle_{vol}$, respectively (for the particulars, the interested reader is referred to [24]). Here, the term "mean particle size" refers to volume averaged particle diameters.

The size distribution spectra in Fig. 6 are non-Gaussian but clearly resemble to log-normal functions. Note that this feature was not obtained by a fit procedure but, rather, is the result of a straightforward calculation.

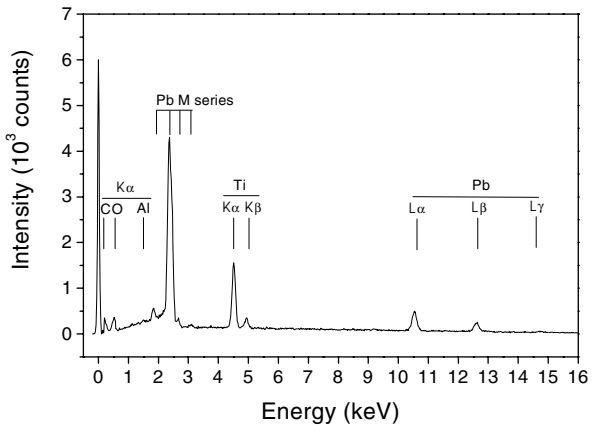

Figure 4 EDX spectrum of $PbTiO_3$ powder sample prepared at 800°C.

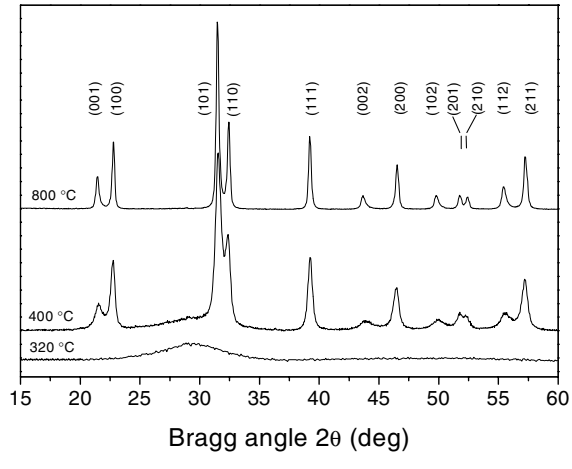

Figure 5 XRD patterns of CPP prepared $PbTiO_3$ powders.

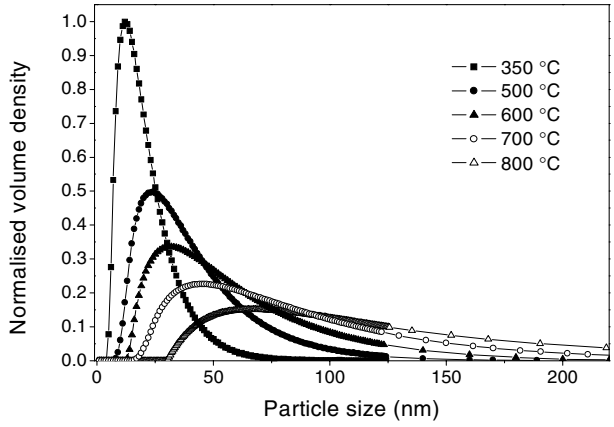

Figure 6 Size distribution spectra (normalized number density) of $PbTiO_3$ powders CPP-prepared at various temperatures.

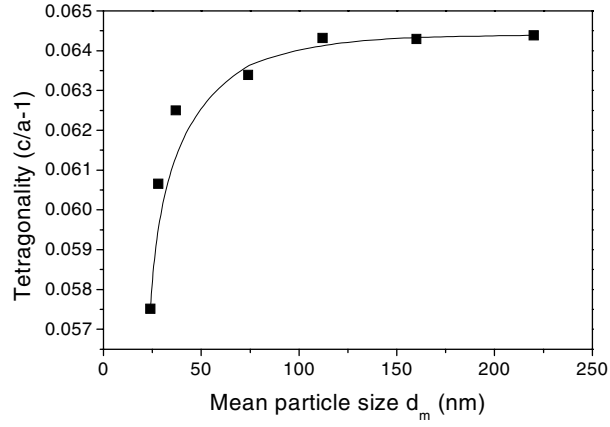

Figure 8 Temperature-dependant tetragonality (c/a−1) as determined from the XRD results for CPP-prepared $PbTiO_3$ powders.

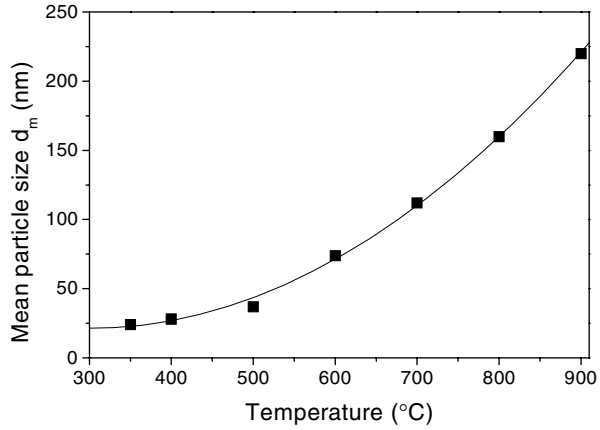

Figure 7 Dependence of mean $PbTiO_3$ particle size d_m on preparation temperature.

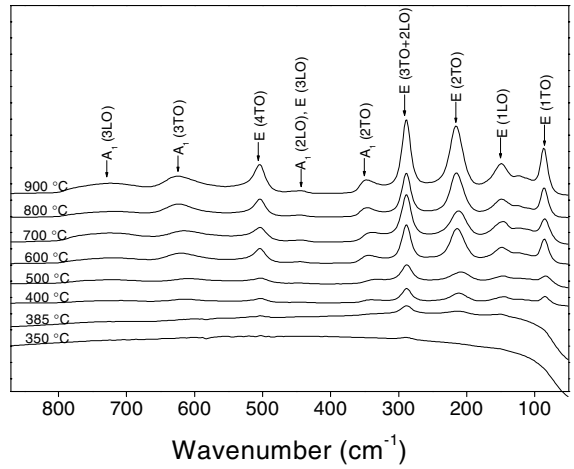

Figure 9 FT-Raman spectra of CPP-prepared $PbTiO_3$ powders.

We should also mention that with growing preparation temperature both mean particle size and distribution width increase (the dependence of the former quantity on preparation temperature is shown in Fig. 7 and reveals quite analogous features to the corresponding finding in preparing $BaTiO_3$ nanopowders [7]).

So far, the $PbTiO_3$ CPP preparation reached a lower size limit of about 20 nm, exceeding the presumable critical size. For further scrutinising the problem of critical size, the tetragonality parameter (c/a−1) was considered in its temperature dependence: The determination of the tetragonal lattice parameters a and c in dependence on the mean particle size was based on the (200) and (002) Bragg reflections. A Voigt-profile fit was applied to determine the Bragg angels of the $K_{\alpha 1}$ and $K_{\alpha 2}$ line components. Then, the peak positions were corrected with respect to the (220) reflection of the internal standard (Si) and the parameters a and c were determined. The size dependence of the tetragonality (c/a−1) in Fig. 8 is highly reminiscent of the corresponding finding obtained earlier for $PbTiO_3$ nanopowders from a coprecipitation route [25], however now indicating a clearly lower critical mean size. Our preliminary EPR spectra reveal well resolved features originating from probe ions on tetragonal and cubic sites, thus disclosing a significant co-existence of cubic and tetragonal powder components. Hence, from our forthcoming EPR studies one can expect a consistent elucidation of the aforementioned apparent discrepancy.

The Raman spectra in Fig. 9 as taken at room temperature from CPP-prepared $PbTiO_3$ nanopowder samples of various mean particle sizes, reveal strong but largely steady changes. The relative continuity is a consequence of the strong stabilisation of the tetragonal ferroelectric phase; for the qualitative spectral differences in rhombohedral, orthorhombic, tetragonal and cubic $BaTiO_3$ phases see, e.g., Fig. 6 in [7]. The symmetry assignment of the Raman lines was taken from a $PbTiO_3$ single crystal spectrum [26] to which that spectrum in Fig. 9 bears the closest resemblance which belongs to the highest preparation temperature and, hence, the largest mean particle size. When going to lower preparation temperature and, consequently, to smaller particle size the Raman bands become increasingly smeared and, finally, disappear. Also red shifts are readily recognizable for various Raman peaks and, particularly the wavenumber shift of the soft mode E(1TO) correlates in Fig. 10 with the pertinent line broadening in the same way as previously reported for sol-gel derived samples [27]. The Raman spectra can well verify both the perovskitic tetragonal $PbTiO_3$ powder material and the relatively wide size range as covered by the CPP route.

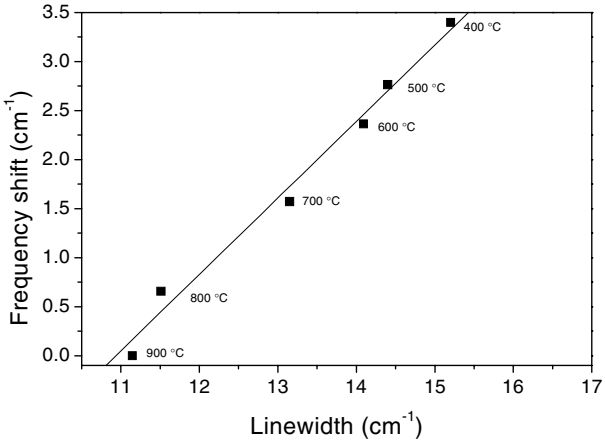

Figure 10 Correlation between linewidth and frequency for the soft E(1TO) vibration band.

The EPR spectra of the chromium doped $PbTiO_3$ nanopowders reveal a superposition of spectra of various paramagnetic centres (cf. Fig. 11). In the $PbTiO_3$ nanopowder sample prepared at 800°C, Cr^{3+} ($S = 3/2$) and Cr^{5+} ($S = 1/2$) ions on Ti^{4+} lattice sites were identified, with spin-Hamiltonian parameters (g factor and fine structure (FS) parameter D) of the Cr^{3+} ions being in accordance with values measured in microcrystalline powders or single crystals [18, 28]. When going to smaller mean particle size all FS lines are broadened and in the 400°C-sample only the central transitions with the spin quantum numbers $M_S = \frac{1}{2} \leftrightarrow -\frac{1}{2}$ are detectable. The broadening effect may be traced back to changes of the FS parameter D due to its dependence on the particle size of the individual nanocrystallite. Additionally, in this sample a new EPR line with $g = 1.974$ occurs which is assigned to Cr^{3+} ions on cubic Ti^{4+} sites, thus indicating a size-driven ferroelectric-to-paraelectric transition into the cubic phase. Hence one can conclude that pronounced size effects occur in the EPR spectra of chromium doped $PbTiO_3$ samples and that CPP-prepared nanopowders of smallest mean particle size contain sufficiently large particle fractions with sizes below the critical value. Nevertheless, application of a micellar route similar to [11] is envisaged to prepare a narrow size distribution mainly lying below critical threshold. Furthermore, forthcoming high-field measurements will point out the size-dependent phenomena in a more pronounced and unambiguous way. These studies will mainly focus on the high-spin case (Cr^{3+} with $S = 3/2$) since for the Cr^{5+} centre ($S = 1/2$) the corresponding size effects can be expected to be rather weak [29].

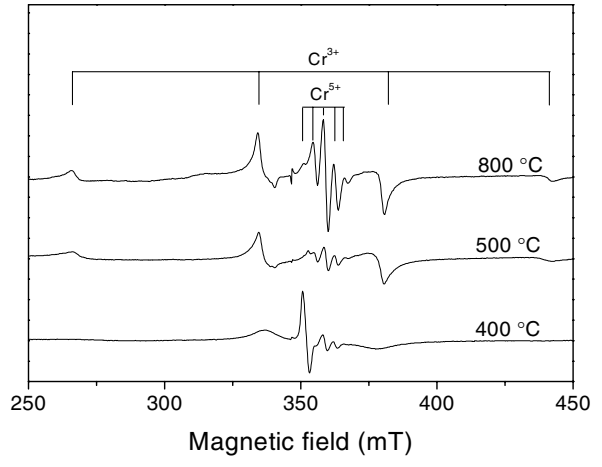

Figure 11 EPR spectra of chromium-doped $PbTiO_3$ powder samples, taken in the X-band.

4. Conclusions

The preparation of $PbTiO_3$ ultrafine powders was achieved by polymerisation of a polynuclear lead titaniumoxy methacrylate as monomeric metallo-organic precursor and consecutive pyrolysis. A particularly advantageous feature of this preparation route is given by the possibility to adjust the particle size in a relatively wide size range by applying appropriate preparation conditions, first of all by choosing adequate reaction temperature. Doping with paramagnetic ions such as Mn^{2+}, Gd^{3+} or Cr^{3+} in a wide concentration range is readily accomplished by just adding the corresponding metal acetates or acetylacetonates to the monomeric precursors. This does not only enable EPR investigations but, moreover, allows for material modification, e.g., with respect to electric conductivity properties of positive temperature coefficient (PTC) or high dielectric constant materials.

The concentration of lattice imperfections and impurities is obviously so low that the correlational length does not fall below geometrical dimension. This renders possible to device a detailed idea of the size-driven structural transformation into cubic paraelectric phase, particularly by employing high-field EPR spectroscopy. In doing so, extension of the particle size range to lower mean values appears feasible by micellar techniques, thus opening a generalised strategy for synthesising metal oxide nanopowders over an extremely wide size range.

Acknowledgement

These investigations were financially supported by *Deutsche Forschungsgemeinschaft* within the priority program *High-field EPR in biology, chemistry and physics.* One of us (E. E.) was granted by *Deutscher Akademischer Austauschdienst* and *Turk Egitim Vakfi*, enabling guest research in Leipzig.

References

1. E. K. AKDOGAN, M. R. LEONARD and A. SAFARI, in "Handbook of Low and High Dielectric Constant Materials," Vol. 2, edited by H. S. Nalwa (Academic Press, San Diego, 1999) p. 61.
2. S. WADA, T. SUZUKI and T. NOMA, *Jpn. J. Appl. Phys.* **34** (1995) 5368.
3. B. MILSCH and R. BÖTTCHER, *Phys. Stat. Sol.* (a) **133** (1992) 455.
4. H.-J. GLÄSEL, E. HARTMANN, R. MEHNERT, D. HIRSCH, R. BÖTTCHER and J. HORMES, *Nucl. Instr. and Meth.* B **151** (1999) 200.
5. H. RUMPF, J. HORMES, H. MODROW, H.-J. GLÄSEL, E. HARTMANN, E. ERDEM and R. BÖTTCHER, *J. Phys. Chem.* B **105** (2001) 3415.
6. R. BÖTTCHER, H.-C. SEMMELHACK, G. VÖLKEL, H.-J. GLÄSEL and E. HARTMANN, *Phys. Rev.* B **62** (2000) 2085.

7. H.-J. GLÄSEL, E. HARTMANN, D. HIRSCH, R. BÖTTCHER, J. HORMES and H. RUMPF, *J. Mater. Sci.* **34** (1999) 2319.
8. D. FU, H. SUZUKI and K. ISHIKAWA, *Phys. Rev.* B **62** (2000) 3125.
9. B. A. HERNANDEZ, K. CHANG, E. R. FISHER and P. E. DORHOUT, *Chem. Mater.* **14** (2002) 480.
10. J. FANG, J. WANG, L. GAN and S. NG, *Mater. Lett.* **52** (2002) 304.
11. S. O'BRIEN, L. BRUS and C. B. MURRAY, *J. Amer. Chem. Soc.* **123** (2001) 12085.
12. T. YOGO, H. UKAI, W. SAKAMOTO and S. HIRANO, *J. Mater. Res.* **14** (1999) 3275.
13. A. R. BABU and A. V. PRASADARAO, *J. Mater. Sci. Lett.* **16** (1997) 313.
14. A. P. BARRANCO, O. P. MARTINEZ and D. K. DAS-GUPTA, *J. Appl. Phys.* **92** (2002) 1494.
15. J. YIN and W. CAO, *ibid.* **92** (2002) 444.
16. Z. YU, C. ANG, R. GUO and A. S. BHALLA, *ibid.* **92** (2002) 1489.
17. F. M. PONTES, E. R. LEITE, D. S. L. PONTES, E. LONGO, E. M. S. SANTOS, S. MERGULHAO, P. S. PIZANI, F. LANCIOTTI, T. M. BOSCHI and J. A. VARELA, *ibid.* **91** (2002) 5972.
18. V. V. LAGUTA, T. V. ANTIMIROVA, M. D. GLINCHUK, I. P. BYKOV, J. ROSA, M. ZARITSKII and L. JASTRABIK, *J. Phys. C: Condens. Matter* **9** (1997) 10041.
19. G. I. DZARDIMALIEVA, A. S. ROZENBERG and A. D. POMAGAILO, *Russ. Chem. Bull.* **44** (1995) 858.
20. J. BRANDRUP and E. H. IMMERGUT, "Polymer Handbook," 3rd ed. (Wiley, New York, 1989) p. V/78.
21. D. BALZAR and H. LEBBETTER, *J. Appl. Cryst.* **26** (1993) 97.
22. S. A. HOWARD and R. L. SNYDER, *ibid.* **22** (1989) 238.
23. D. BALZAR, *J. Res. Natl. Inst. Stand. Technol.* **98** (1993) 321.
24. C. E. KRILL and R. BIRRINGER, *Philos. Mag.* A **77** (1998) 621.
25. S. CHATTOPADHYAY, P. AYYUB, V. R. PALKAR and M. MULTANI, *Phys. Rev.* B **52** (1995) 13177.
26. G. BURNS and B. A. SCOTT, *ibid.* **7** (1973) 3088.
27. W. MA, M. ZHANG and Z. LU, *Phys. Stat. Sol.* (a) **166** (1998) 811.
28. R. HEIDLER, W. WINDSCH, R. BÖTTCHER and C. KLIMM, *Chem. Phys. Lett.* **175** (1990) 55.
29. R. BÖTTCHER, W. BRUNNER, B. MILSCH, G. VÖLKEL, W. WINDSCH and S. T. KIRILLOV, *ibid.* **129** (1986) 546.

Received 5 November 2002
and accepted 18 April 2003